Dalton Transactions

Accepted Manuscript

ROYAL SOCIETY OF CHEMISTRY

www.rsc.org/dalton

B-site ordered double perovskite $LaBa_{1-x}Sr_xZnSbO_6$ ($0 \leq x \leq 1$): Sr^{2+}-doping induced symmetry evolution and structure-luminescence correlations

Pengfei Jiang, Zhengyang Zhou, Wenliang Gao, Rihong Cong, Tao Yang**

College of Chemistry and Chemical Engineering, Chongqing University, Chongqing 400044, P. R. China

*Correspondence authors, email: congrihong@cqu.edu.cn; taoyang@cqu.edu.cn.

Tel: (8623)65105065, Fax: (8623)65105065.

Abstract

The study of perovskites has been active for a long time. Here we rationally designed and prepared a double perovskite $LaBaZnSbO_6$ by selecting Zn^{2+} and Sb^{5+} with large size and charge differences, and indeed, the complete B-site ordering can be achieved. Careful study on powder X-ray diffraction data pinpointed its space group to be $I2/m$, which was rarely seen in double perovskites. Thereafter, an interesting observation of Sr^{2+}-doping induced symmetry evolution from $I2/m$ to $P2_1/n$ was confirmed in the complete solid solutions $LaBa_{1-x}Sr_xZnSbO_6$, where the tilting system also transferred from $a^-a^-c^0$ to $a^-a^-c^+$. The transition boundary is around $x = 0.4$. It can also be visualized by the variation of θ (defined as $c/[(a+b)/2]$), which is associated with the anisotropic shrinkage of the unit cell lattice and indeed shows a minimum at $x = 0.4$. Such a successive modulation of both the structure symmetry and the average La/Ba/Sr-O bond distances (revealed by Rietveld refinements) motivated us to study the Eu^{3+}-luminescence in $La_{0.95}Eu_{0.05}Ba_{1-x}Sr_xZnSbO_6$. Interestingly, the maxima of charge transfer absorption of Eu^{3+} shows a precise changing tendency with the A-O bond distances along with the Sr^{2+}-doping, clearly revealing the structure-luminescence correlations.

Keywords: double perovskites; powder X-ray diffraction; Rietveld refinements; luminescence; structure-luminescence correlations.

Introduction

Perovskites with the general formula ABO_3 represent a large family in solid state chemistry. Perovskite-type structure is able to accommodate various elements covering a wide range of ionic size and charge, which gives rise to a great structure diversity. Thus physical properties for perovskite and perovskite-relate materials cover almost every aspect, such as ferroelectricity,[1-3] superconductivity,[4-5] ferromagnetism,[6] ionic conductivity[7] and so on. As is well known, the physical properties for ABO_3-perovskites strongly rely on the electronic configurations of A- and/or B-cations. In order to design or modulate the physical properties, chemists can rationally synthesize so-wanted compositions. The recent discovery of room temperature multiferroics by Rosseinsky M.J. and his coworkers is a typical example. During the preparation of solid solutions, they carefully manipulated the relative ratio between two perovskite-related end members, $(Ca_ySr_{1-y})_{1.15}Tb_{1.85}Fe_2O_7$ (y = 0.60 and 0.563) and $Ca_3Ti_2O_7$, where the former is non-polar but antiferromagnetic at room temperature and the latter one is a polar oxide, they eventually obtained an electrical polarization and magnetization above the room temperature simultaneously.[8]

Double perovskites with the general formula $AA'BB'O_6$ or $A_2BB'O_6$ show the A- and/or B-sites ordering, which would extend the pristine framework to a super lattice. Sometimes, the cation ordered materials exhibit special physical behaviors which may be significantly different from the disordered materials, like the case that the B-site ordering perovskite Sr_2FeMoO_6 exhibits colossal magnetoresistance behavior.[9] The driving forces for the cationic ordering in double perovskite include the size and charge differences.[10, 11] Up to now, three types of B-site ordering were observed such as rock-salt, columnar and layered ordering.[10, 12] Among them, the rock-salt ordering is most commonly seen. Herein, we used Zn^{2+} (r = 0.74Å, in 6-coordination) and Sb^{5+} (r = 0.6Å) in B-sites,[13] which offers a relatively large size and charge differences. $LaBaZnSbO_6$ was prepared by typical solid state reactions, and as expected, a complete rock-salt ordering was observed in the monoclinic space group $I2/m$. In addition, the octahedra tilting and rotation behaviors can be modulated by rationally doping Sr^{2+} into

the A-site, for example, a symmetry lowering was confirmed from *I*2/*m* to *P*2/*n* in $LaBa_{1-x}Sr_xZnSbO_6$ ($0 \leq x \leqslant 1$) by careful Rietveld refinements together with luminescence study. It is interesting to find that the changing tendency of Eu^{3+}-luminescence was precisely consistent with the evolution of A-O bond distances along the Sr^{2+}-doping.

Experimental

The polycrystalline samples $LaBa_{1-x}Sr_xZnSbO_6$ ($0 \leq x \leq 1$) were prepared by traditional solids state reactions. Lanthanum oxide (La_2O_3, Founder star science & technology, Beijing, 99.99%), barium carbonate ($BaCO_3$, Alfa Aesar, 99.8%), strontium carbonate ($SrCO_3$, Alfa Aesar, 99.8%), zinc oxide (ZnO, Alfa Aesar, 99.9%) and antimonic oxide (Sb_2O_3, Alfa Aesar, 99.9%) were used as starting materials. Stoichiometric amounts of the starting materials were weighted and mixed in the agate mortar and then heated at 600°C over night to ensure the completely oxidation of Sb^{3+} into Sb^{5+}. Subsequently, the resulting powers were heated at 900°C for 10h. After this calcination, the powder were pressed into pellets and annealed at 1200~1250 °C (depending on the compositions) for 60 h with several intermediate grindings to obtain the final pure phases of $LaBa_{1-x}Sr_xZnSbO_6$. Moreover, europium oxide (Eu_2O_3, Founder star science & technology, Beijing, 99.99%) was used as europium source for preparing Eu^{3+} doped samples $La_{0.95}Eu_{0.05}Ba_{1-x}Sr_xZnSbO_6$ ($0 \leq x \leq 1$) and $La_{1-y}Eu_ySrZnSbO_6$ (y = 0.025, 0.05, 0.08). And the Eu^{3+} doped samples were prepared with same procedure and finally heated at 1250 °C for 20 h.

The phase purity of the final sample was checked by X-ray diffraction (XRD) performed on the diffractometer equipped with a PXIcel 1D detector (Cu Kα radiation). The operation voltage and current are 40KV and 40mA, respectively. The data used for phase identification were collected with a setting of 30 s / 0.0262 º. High quality XRD data, which were used for Rietveld refinements, were collected with a setting of 200 s / 0.0131 º. Rietveld refinements were performed using the TOPAS software package.[14]

The rotation electron diffraction (RED) data of $LaBaZnSbO_6$ were collected on a JEOL JEM2100 TEM with very dose electron beam by using the second condenser aperture.[15-17] A single tilt sample holder with ±35° goniometer tilt was used. The TEM and camera were controlled by the RED program automatically and electron diffraction patterns were recorded by a Gatan ES500W Erlangshen camera. The datasets were collected with the tilt angle range from -22.48 to -3.63° for $LaBaZnSbO_6$. The exposure time is 1.5 s for each frame and in total 120 frames were recorded, which were then used to construct the reciprocal space for the data reduction.

Results and Discussion

Symmetry identification

The samples $LaBa_{1-x}Sr_xZnSbO_6$ ($0 \leq x \leq 1$) were obtained as white powder and their XRD patterns are present in Fig. 1a. With increasing doping content of Sr^{2+}, the diffraction peaks slightly shift to higher angles which consistent with the smaller ionic size of Sr^{2+} (1.44 Å in 12-coordination) by comparison with Ba^{2+} (1.61 Å).[13] As shown in Fig. 1a, the diffraction peaks at~19°, ~37 °and 49° are apparent and typical for a perovskite with B-site superstructure, i.e. their indices are (111), (311) and (331) in a face-centered cubic unit cell. At the very beginning, we assigned the space group of $LaBaZnSbO_6$ to *Fm*-3*m*, which is widely adapted by 1:1 ordered double perovskites with the tolerance factor close to 1. For example, the tolerance factor of $LaBaZnSbO_6$ was estimated to be 0.98 by $t = \langle A\text{-}O\rangle/\sqrt{2}\langle B\text{-}O\rangle$ (La^{3+}, 1.36 Å, Ba^{2+}, 1.61 Å, Zn^{2+}, 0.74 Å, Sb^{5+}, 0.60 Å, and O^{2-}, 1.40 Å).[13] By closely looking at the XRD pattern of $LaBaZnSbO_6$, we observed the peak splitting at ~38.6 °(with the index of $(111)_p$, the subscript p means the prototype perovskite structure in the space group *Pm*-3*m*) and at 44.9 °(with the index of $(002)_p$) as shown in Fig. 1b. Such a peak splitting is more obvious for the Sr-doped samples with x = 0.2 and 0.4. Accordingly, the cubic and tetragonal space groups of *Fm*-3*m* and *I*4/*m* are ruled out and the real symmetry of $LaBa_{1-x}Sr_xZnSbO_6$ should be lowered to monoclinic. In fact, the general principles on crystal symmetry for B-site ordered double perovskites were proposed by Woodward and his co-workers, where the allowed space groups in monoclinic system include *C*2/*c*, $P2_1/c$ and *C*2/*m* (*I*2/*m*

with a different original choice).[18] Here, we found that the most possible space group for $LaBa_{1-x}Sr_xZnSbO_6$ ($x \leq 0.4$) is *I*2/*m*, though it is rarely seen, i.e. only a few Sb^{5+} based B-site ordered perovskites ($LaBaMSbO_6$, $M = Cu^{2+}$, Mn^{2+}, Ni^{2+}) adapt this symmetry.[19-21] With further increasing the Sr^{2+} content ($x \geq 0.6$), a group of new peaks appear which could not be fitted with *I*2/*m*. This phenomenon usually suggests a symmetry lowering. And indeed, these new peaks could be indexed with $h + k + l = 2n + 1$ using the same unit cell parameters (see Fig. 1c), which were allowed by the space group $P2_1/n$.[18]

In order to further confirm the symmetry of $LaBaZnSbO_6$, the RED method was then employed to collect the electron diffraction data. The selected planes of the reciprocal lattice corresponding to 1*kl* and 2*kl* were shown in Fig. S1. The reflection conditions in 1*kl* and 2*kl* planes could be obtained with $1 + k + l = 2n$ and $2 + k + l = 2n$, which further indicates it has the reflection condition with $h + k + l = 2n$. Therefore, the space group of $LaBaZnSbO_6$ should be *I*2/*m*.

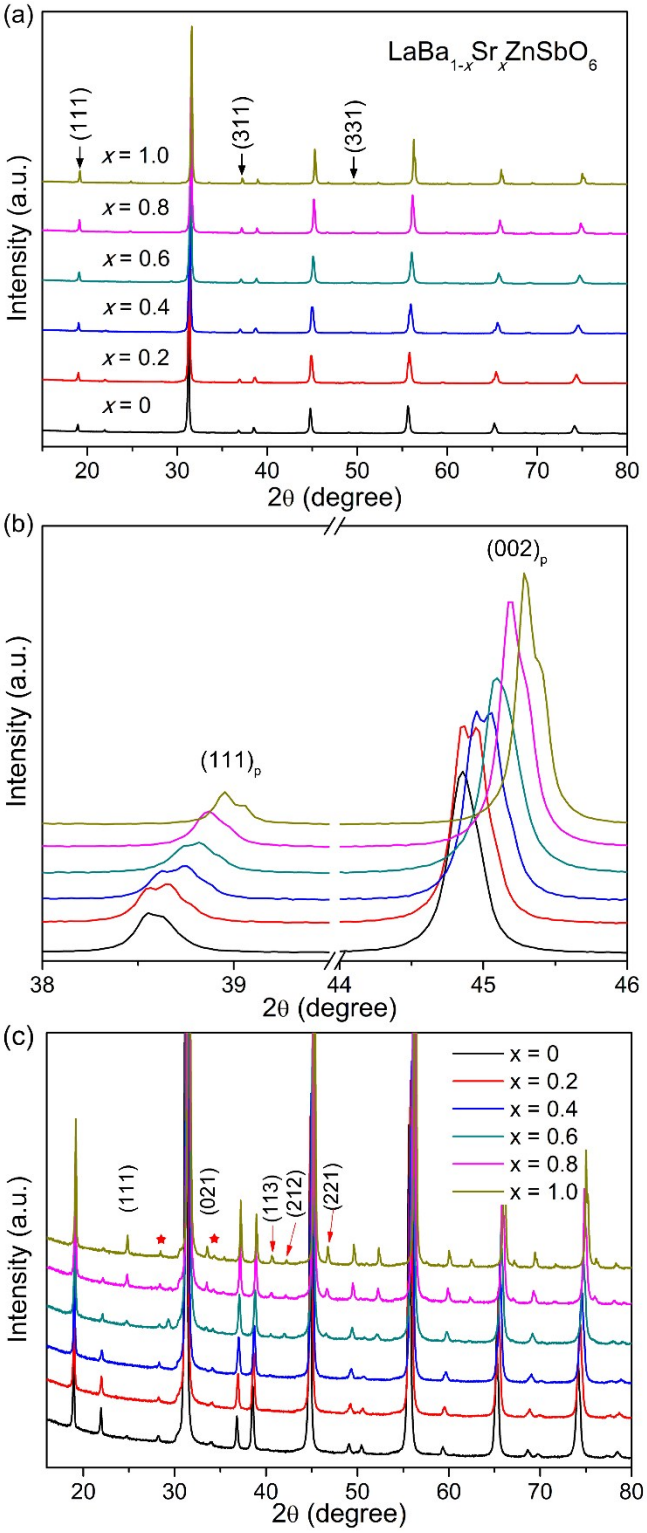

Fig. 1 (a) XRD patterns for $LaBa_{1-x}Sr_xZnSbO_6$; (b) splitting of characteristic peaks; (c) a group of new peaks ($h + k + l = 2n + 1$) emerge by increasing the Sr^{2+}-substitution content ($x \geqslant 0.6$). Note that a small amount of La_3SbO_7 impurity was present and the reflection peaks are highlighted as red stars.

XRD patterns for $La_{1-y}Eu_ySrZnSbO_6$ (y = 0.025, 0.05, 0.08) were given in Fig. S2 in the Electronic Supplementary Information, ESI. The XRD patterns for $La_{0.95}Eu_{0.05}Ba_{1-x}Sr_xZnSbO_6$ were similar with their corresponding hosts $LaBa_{1-x}Sr_xZnSbO_6$, indicating no change of structure symmetry by such a small doping content of Eu^{3+}. The lattice parameters were obtained by Le-Bail fitting and given in Table S1, ESI. The slightly smaller cell volumes for Eu^{3+} doped samples, by comparison with their hosts, attribute to the relative smaller ionic size of Eu^{3+} comparing with La^{3+}, which further support the successful doping of Eu^{3+} into the host lattice.

Rietveld Refinements and Structural evolution

Detailed structural evolutions were analyzed by careful Rietveld refinements on all the title compounds. As described above, the strong superstructure diffraction peaks at~19º, ~37 ° and 49º indicates the presence of rock-salt type ordering of B-site cations.[22] During the refinement process, the occupancies of A-site cations were fixed to be the same with the initial ones. In order to check the possibility of any anti-site Zn^{2+}/Sb^{2+} disordering, the occupancies of Zn^{2+}/Sb^{2+} at two independent B-sites were refined for all samples. It turned out that the largest anti-site Zn^{2+}/Sb^{2+} disordering was 2.5% in $LaBaZnSbO_6$, and this is a strong indication of the fully B-site ordering within the experimental error. Thereafter, the completely B-site ordered structure model was applied in the following refinements. The final convergences of Rietveld refinements for $LaBa_{1-x}Sr_xZnSbO_6$ ($0 \leq x \leq 1$) were given in Figs. 2 and S3, ESI. The very good agreements between the experimental and calculated data (together with very low agreement factors) confirmed that the completely B-site ordering model was correct. The atomic coordinates obtained from the Rietveld refinements with the completely ordering model are given in Tables 1 and S2, ESI. The selected interatomic distances are also presented in Tables 2 and S3, ESI.

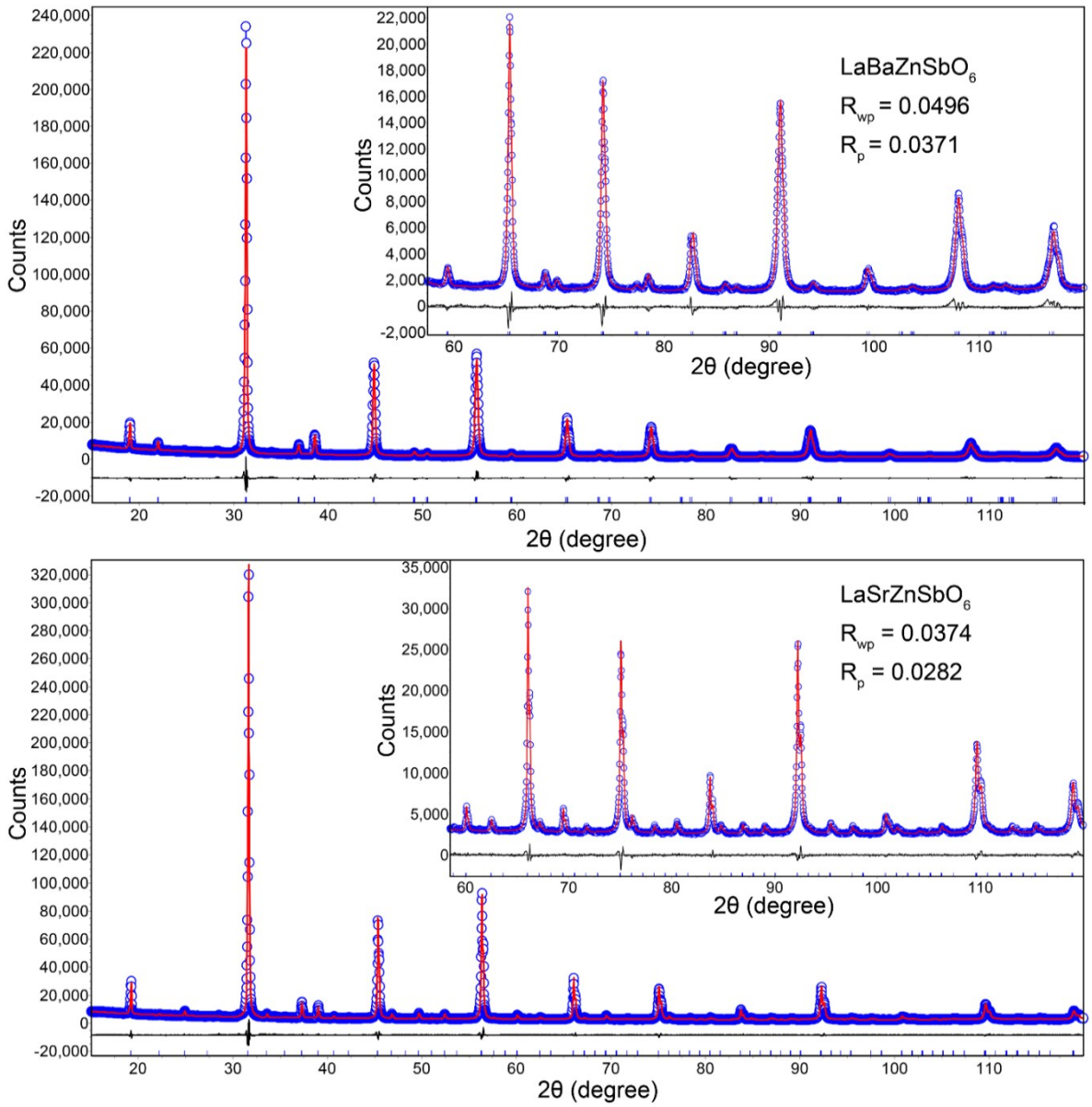

Fig. 2 Final convergences of Rietveld refinements for $LaBaZnSbO_6$ (top) and $LaSrZnSbO_6$ (bottom). The blue symbol ○ represents observed data and the red solid line is the calculated pattern; the blue marks below the diffraction patterns are the expected reflection positions, and the difference curve is also shown at the bottom. Enlargements of the high angle part are shown in the top-right corner.

The unit cell parameters obtained from the Rietveld refinements were plotted along with the Sr^{2+}-content (see Fig. 3) and given in Table S4. With the increasing Sr^{2+}-content, the cell parameters and the average <A-O> bond distances monotonously decrease. Such a behavior is consistent with the smaller ionic of Sr^{2+} and the evolution of the XRD patterns. We note that the values of β for all samples were

very close to 90°. Attempts to refine the structure in an orthorhombic space group were all unsuccessful. Consequently, we could conclude that the symmetry of the atomic arrangements within the unit cell is monoclinic, although the unit cell is close to orthorhombic. Please note that there is a fast decrease of average <A-O> bond distance at the last point in Fig. 3b, which will be further discussed in later sections.

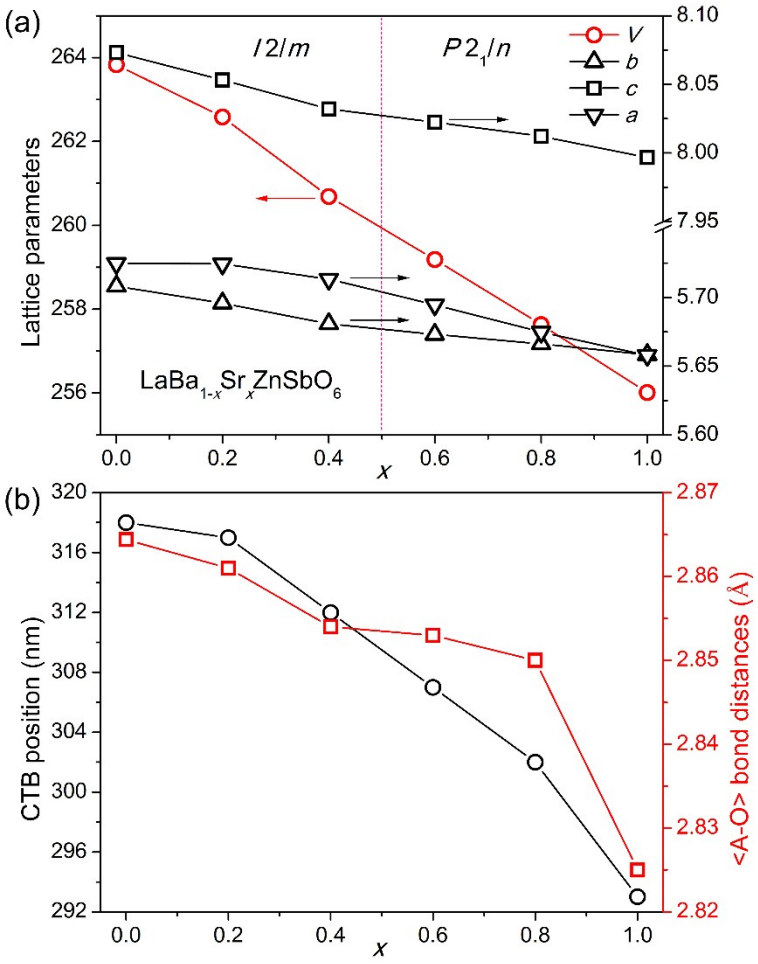

Fig. 3 (a) Evolution of lattice parameters and (b) average <A-O> bond distances for $LaBa_{1-x}Sr_xZnSbO_6$ versus the doping content of Sr^{2+}.

The crystal structures of $LaBaZnSbO_6$ and $LaSrZnSbO_6$ were shown in Fig. 4. Differently, $LaBaZnSbO_6$ and $LaSrZnSbO_6$ possess $a^-a^-c^0$ and $a^-a^-c^+$ tilt systems, respectively, which were consistent with the Glazer's notation.[23] Both $a^-a^-c^0$ and $a^-a^-c^+$ tilt systems were suitable for 1:1 B-site ordering in rock-salt type ordering. The tilt of the octahedra was induced by the smaller A-site cations, which is helpful for improving the coordination environment. In addition, the tilting of the octahedra

would lead to the Zn-O-Sb bond angles smaller than 180°. Consequently, the distortion of the structure could also be exhibited by the tilting angle (Φ) of the octahedra. The average tilting angle of the ZnO_6 and SbO_6 octahedra could be calculated with the formula $\Phi = (180-\psi)/2$, where ψ represents the average band angle of Zn-O-Sb. As shown in Fig. 5a, the tilting angles of $LaBa_{1-x}Sr_xZnSbO_6$ increase along with the content of Sr^{2+}. The evolution of tilting angles indicates that the structure distortion increases as Sr^{2+} doped into the lattice.

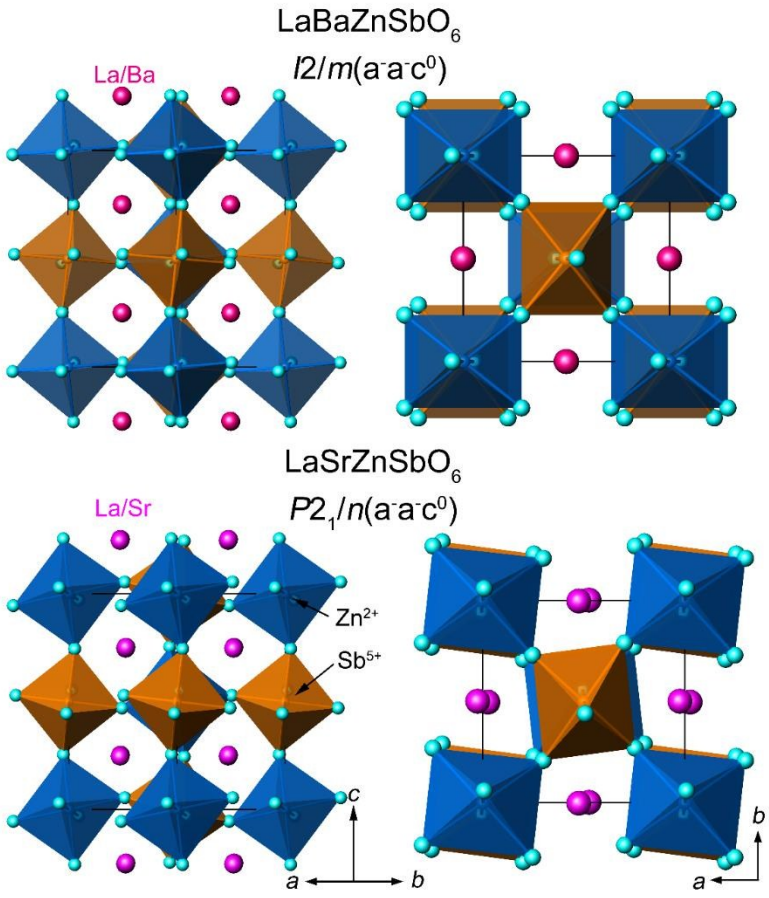

Fig. 4 Crystal structure views along the [110] (left) and [001] (right) directions for the completely B-site ordered perovskites $LaBaZnSbO_6$ and $LaSrZnSbO_6$. Blue and brown octahedra represent ZnO_6 and SbO_6, respectively. La/Ba/Sr cations are shown as purple spheres.

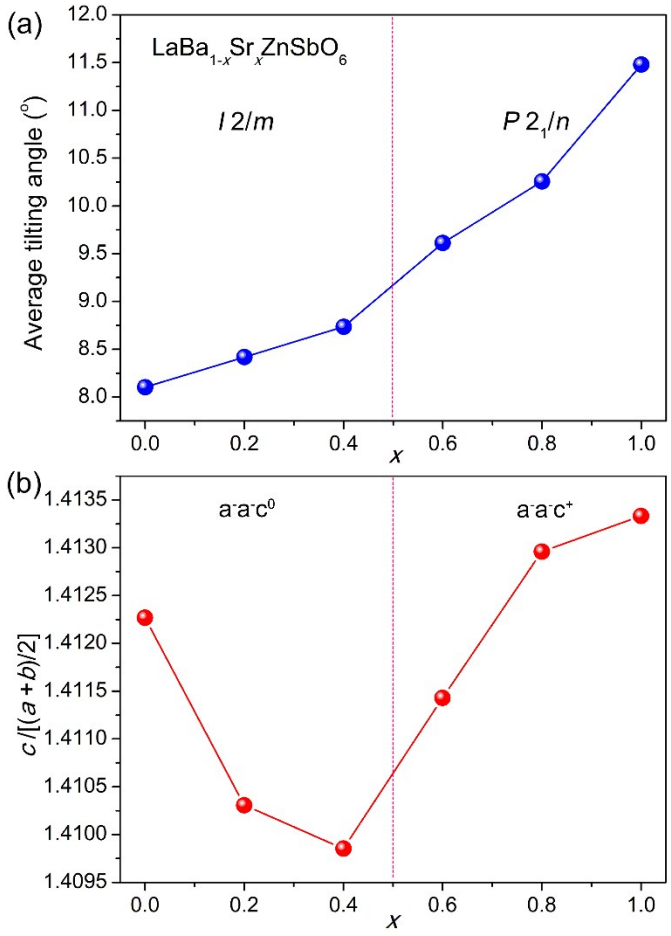

Fig. 5 (a) Average tilting angles and (b) the values of θ (defined as c/[(a+b)/2]) along with the doping content of Sr^{2+}.

Moreover, the different tilt system of the sample $LaBa_{1-x}Sr_xZnSbO_6$ would result in an anisotropic shrinkage of the lattice. In order to better understand this behavior, we plotted the values $\theta = c/[(a+b)/2]$ versus the content of Sr^{2+}, where *a*, *b* and *c* were the lattice parameters of $LaBa_{1-x}Sr_xZnSbO_6$. As shown in Fig. 5b, the θ values of all the samples deviate from ideal value ($\sqrt{2}$), which attributes to the structural distortion. First, θ decreases in the range of $x \leq 0.4$ and then increases. This behavior is apparently related to the change of the tilt system. For detail, in $LaBa_{1-x}Sr_xZnSbO_6$ ($x \leq 0.4$) with the space group *I*2/*m*, both anti-tilts along the *a*- and *b*-axes would result in the more significant shrinkage of the *c*-axis length ($\Delta c = 0.041$ Å) than other two directions ($\Delta a = 0.019$ Å, $\Delta b = 0.028$ Å). Consequently, θ decreases within the range of $x \leq 0.4$. In the following ($x \geq 0.6$), the emergence of c^+ tilt in the space group $P2_1/n$ would only lead to the shrinkage of *a* and *b* parameters, where the shrinkage of *c*-axis length ($\Delta c = 0.026$

Å, caused by the substitution of smaller cations) is much smaller than that of *a*- and *b*-axis (Δa = 0.037 Å, Δb = 0.148 Å). So, an increase of θ was observed for $x \geq 0.6$. The reorientation of the tilts of the octahedra always leads to the reversal of the pseudo-cubic *c*/*a* values, which is observed in numerous perovskites.[24] In our case, the variation of θ values is due to the structure symmetry change from *I*2/*m* ($a^-a^-c^0$) to $P2_1/n$ ($a^-a^-c^+$). From this aspect, the evolution of θ could reflect the tilt system change in $LaBa_{1-x}Sr_xZnSbO_6$ ($0 \leq x \leq 1$), which again confirms the selected space groups for structure refinements are correct.

According to the refinements, both Zn^{2+} and Sb^{5+} located in slightly distorted octahedral cavities (refer to Tables 1 and S2). The average bond distances of Zn-O is larger than that of Sb-O, which agrees well with the ionic size difference between Zn^{2+} and Sb^{5+} (0.74 Å and 0.6 Å for Zn^{2+} and Sb^{5+}, respectively).[13] The average Sb-O bond distances in all compounds are almost unchanged, which are comparable with the observed bond distances in Sb_2O_5 (1.992 Å)[22] and Pb_2TmSbO_6 (1.98 Å).[26] In general, B-site ordering in double perovskites was induced by large size and charge differences. In $La(Ba/Sr)Zn^{2+}Ta^{5+}O_6$ and $LaSrNi^{2+}Sb^{5+}O_6$, only a partial ordering was observed.[27, 28] This may attribute to the ionic size difference is relatively smaller (0.1 Å and 0.09 Å for $La(Ba/Sr)ZnTaO_6$ and $LaSrNiSbO_6$, respectively). Herein $LaBa_{1-x}Sr_xZnSbO_6$, the size and charge difference between Zn^{2+} and Sb^{5+} were 0.14 Å and three, respectively, which is large enough to induce a complete B-site ordering. Moreover, the rock-salt type ordering of Zn^{2+} and Sb^{5+} in $LaBa_{1-x}Sr_xZnSbO_6$ was in good agreement with the calculated band valence sums (BVS) of Zn^{2+} and Sb^{5+} (see Tables 2 and S3).

Luminescence study of $La_{0.95}Eu_{0.05}Ba_{1-x}Sr_xZnSbO_6$ ($0 \leq x \leq 1$) and $La_{1-y}Eu_ySrZnSbO_6$ (y = 0.025, 0.05, 0.08)

In recent years, the white light-emitting diodes (LEDs), represents so-called next generation sold state lighting, which has received considerable attention duo to its reliability, energy saving, maintenance and safety. Currently, the most common approach to produce white light is to combine a blue LED chip with a yellow phosphor (YAG: Ce^{3+}).[29] While this type of white light has poor color

rendering caused by the color deficiency in red and blue-green of phosphors. The alternative way to achieve white light is touse a UV LED with RGB (red, green, blue) phosphor, or coupling a blue LED to RG phosphors. For these routes, the red phosphor which could be efficiently excited by the GaN and InGaN chips are in great demand. Herein, the photoluminescent properties of Eu^{3+} doped $LaBa_{1-x}Sr_xZnSbO_6$ red emission phosphors were studied by using Eu^{3+} as a site symmetry probe to further confirm the correction of the structure symmetry of $LaBa_{1-x}Sr_xZnSbO_6$.

The excitation spectra of $La_{0.95}Eu_{0.05}Ba_{1-x}Sr_xZnSbO_6$ were measured from 250 to 500 nm by monitoring the strongest Eu^{3+} emission at 617 nm, as shown in Fig. 6a. All of the excitation spectra show similar profiles, which consist of an intense broad band in the shorter wavelength region (250-350 nm) and several groups of sharp peaks in the longer wavelength region (350-550 nm). Obviously, the sharp peaks in the region of 350-550 nm is the characteristic *f-f* transitions of Eu^{3+} ions, whose positions are almost unchanged along with the doping content of Eu^{3+} duo to the inert nature for *f-f* transitions.[30, 31] On the contrary, the broad band attributes to the charge transfer (CT) from O^{2-} to Eu^{3+} and shows a significant blue shift from 319 nm for $x = 0$ to 295 nm for $x = 1.0$, together with the increasing of the absorption intensity. Since the CT excitation is an electronic transition, and the band position is corresponding to the Eu^{3+}-O^{2-} bond co-valency. Usually, the increase of the co-valency would induce a blue shift of the CT band. By Sr^{2+}-doping, the average <A-O> bond distance declines against the doping content x (see Fig. 3b), which of course leads to the increase of the Eu^{3+}-O^{2-} co-valency. As a result, a blue shift of about 25 nm was observed for $La_{0.95}Eu_{0.05}Ba_{1-x}Sr_xZnSbO_6$ ($0 \leq x \leq 1$), which interestingly shows a well-match with the <A-O> bond distances (see Fig. 3b). Additionally, the absorbance of CT band are much higher than that of *f-f* transitions and all of them show an increase tendency along with x, which further indicates the crystal-field around Eu^{3+} was modified by Sr^{2+} doping.

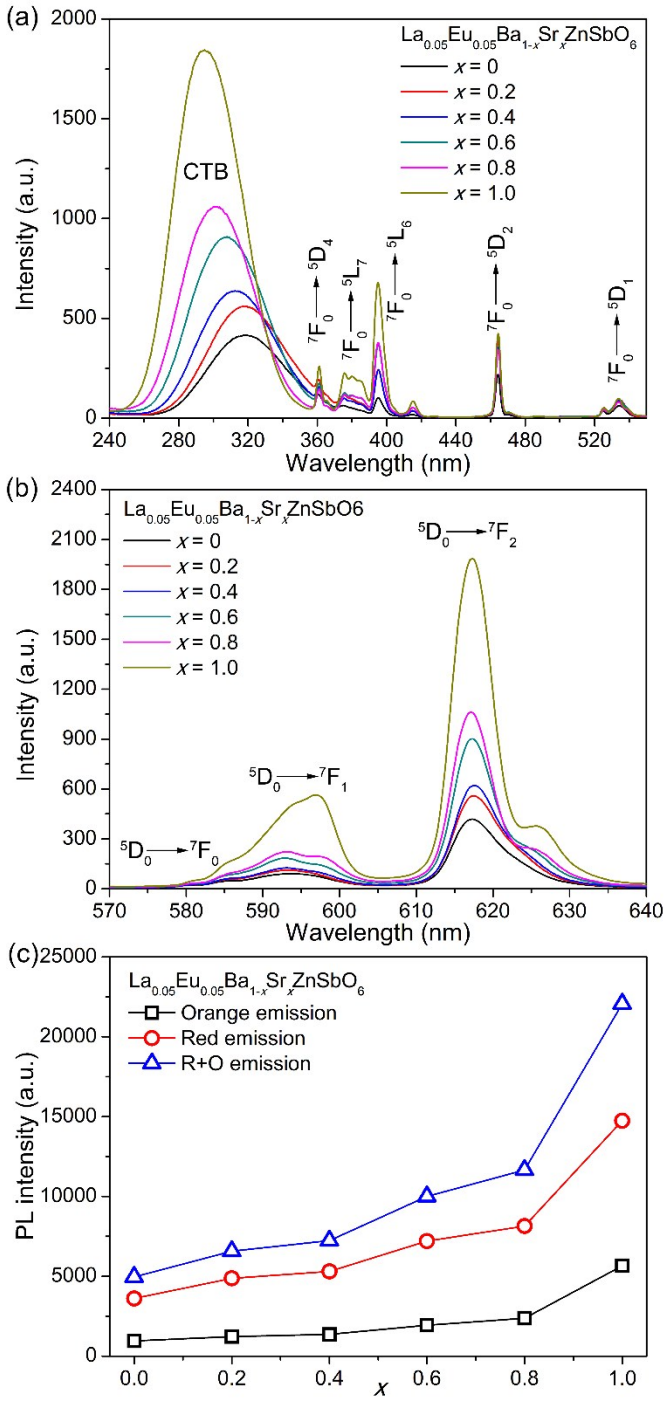

Fig. 6 (a) Excitation spectra of $La_{0.95}Eu_{0.05}Ba_{1-x}Sr_xZnSbO_6$ by monitoring the emission at 617 nm of Eu^{3+}; (b) emission spectra of $La_{0.95}Eu_{0.05}Ba_{1-x}Sr_xZnSbO_6$ excited by the charge transfer (CT) of O^{2-}-Eu^{3+}. (c) variations of $^5D_0 \rightarrow {}^7F_1$, $^5D_0 \rightarrow {}^7F_2$ and total emission intensities of $La_{0.95}Eu_{0.05}Ba_{1-x}Sr_xZnSbO_6$ along with the content of Sr^{3+}.

Moreover, as shown in the Fig. 6a, $La_{0.95}Eu_{0.05}Ba_{1-x}Sr_xZnSbO_6$ could be excited not only by ultraviolet or near-ultraviolet light but also by blue ($^7F_0 \rightarrow {}^5D_2$, 465 nm) and green ($^7F_0 \rightarrow {}^5D_1$, 535 nm) irradiations, which could match the blue light from the InGaN chips. Additionally, it is rarely seen about the relative strong $^7F_0 \rightarrow {}^5D_2$ absorption, unlike many reported materials.[32] Particularly in $La_{0.95}Eu_{0.05}BaZnSbO_6$, $^7F_0 \rightarrow {}^5D_2$ is the strongest among all the *f-f* transitions. As Sr^{2+} doped into the lattice, $^7F_0 \rightarrow {}^5L_6$ eventually become the dominant transitions. The evolution of the relative intensity for *f-f* transitions further consolidates the change of crystal-field strength around Eu^{3+}. The strong $^7F_0 \rightarrow {}^5D_2$ transition was also observed in the Sb^{5+} containing B-site ordered perovskite $Ca_2LaSbO_6:Eu^{3+}$ in which the $^7F_0 \rightarrow {}^5D_2$ transition was the strongest among the excitation spectra.[33] Although $La_{0.95}Eu_{0.05}Ba_{1-x}Sr_xZnSbO_6$ could be excited by the blue InGaN chips, the intensity of blue light are relatively low by comparison with other nitrides i.e. Eu^{2+} $CaAlSiN_3$,[34] because the 4f-5d transition of Eu^{2+} is very sensitive to the crystal field and co-valency, Eu^{2+}-doped phosphors have a strong absorption from the UV to the visible region.

The compositional dependent photoluminescence (PL) emission spectra are presented in Fig. 6b, which were record in the range of 570-640 nm under the excitation of CTB (charge transfer from O^{2-} to Eu^{3+}). Three groups of emission peaks at 581, 585-605, and 610-635 nm were observed, which are readily attributed to the $^5D_0 \rightarrow {}^7F_J$ (J = 0, 1, 2) transitions of Eu^{3+}, respectively.[27] The $^5D_0 \rightarrow {}^7F_0$ (at 581 nm) is a single peak for all the samples, as there is only one crystallographic site in $La_{0.95}Eu_{0.05}Ba_{1-x}Sr_xZnSbO_6$ no matter the structure symmetry is *I*2/*m* or $P2_1/n$. The total intensity of emission peaks corresponding to $^5D_0 \rightarrow {}^7F_1$ transitions is much weaker than that of $^5D_0 \rightarrow {}^7F_2$ transitions. It is well known that $^5D_0 \rightarrow {}^7F_1$ and $^5D_0 \rightarrow {}^7F_2$ is the magnetic dipole-dipole and electronic dipole-dipole transitions, respectively. The latter ($^5D_0 \rightarrow {}^7F_2$) is very sensitive to the local symmetry of Eu^{3+}, which would be the dominant emission when Eu^{3+} deviates from the inversion center. As shown in Fig. 6b, the much stronger $^5D_0 \rightarrow {}^7F_2$ emissions indicate that Eu^{3+} locates at a non-centrosymmetric position in

$La_{0.95}Eu_{0.05}Ba_{1-x}Sr_xZnSbO_6$, which is really consistent with the monoclinic structure type of the title compounds.

The calculated $^5D_0 \rightarrow ^7F_1$ (orange light), $^5D_0 \rightarrow ^7F_2$ (red light) and total emission intensities along with *x* are presented in Fig. 6c. The intensities of orange and red emission both increase with the content of Sr^{2+}. Note that all the samples in $La_{0.95}Eu_{0.05}Ba_{1-x}Sr_xZnSbO_6$ have the same content of Eu^{3+} and prepared with the same procedure. Thus, we can conclude that the increase of PL intensity attributes to the local structure modification of Eu^{3+} induced by doping smaller Sr^{2+}. This phenomenon is consistent with the evolution of the tilting angle which indicates the structure distortion increase along with Sr^{2+} content (see Fig. 3b). It is worthy mention that the final significant increase of the emission intensity (see Fig. 6c) is consistent with the final fast decrease of the average <A-O> bond distance shown in Fig. 3b. Moreover, it is well known that the Red/Orange (*R*/*O*) = I($^5D_0 \rightarrow ^7F_2$)/ $^5D_0 \rightarrow ^7F_1$ is recognized as the probe of site symmetry of Eu^{3+}. The calculated *R*/*O* ratios for the samples are ~3.5 indicating Eu^{3+} locates at a non-centrosymmetric site (see Tables 2 and S3, ESI), which is consistent with the site symmetry of A-site cations in $LaBa_{1-x}Sr_xZnSbO_6$. The site symmetry of the A-site cations was lowered from C_s to C_1 by Sr^{2+} doping. Moreover, the site symmetry lowering of Eu^{3+} also benefits to the increase of the emission intensities of $La_{0.95}Eu_{0.05}Ba_{1-x}Sr_xZnSbO_6$. These results further consolidate that the choice of *Fm*-3*m* or *I*4/*m* is inappropriate for $LaBa_{1-x}Sr_xZnSbO_6$, because A-site cations would have located at the centrosymmetric site in such a cubic or tetragonal symmetry.

The compositional dependent PL luminescence of $La_{0.95}Eu_{0.05}Ba_{1-x}Sr_xZnSbO_6$ excited by 394nm (*f*-*f* transition of Eu^{3+}) were also studied. The PL emission spectra and calculated total emission intensity are presented in Fig. S4, ESI. The emission spectra show similar profiles but with lower intensities comparing with those being excited by CTB. The total emission intensities increase along with the content of Sr^{2+}. Moreover, we also performed the PL study for $La_{1-y}Eu_ySrZnSbO_6$ (y = 0.025, 0.05, 0.08) in order to confirm that the PL emission evolution in $La_{0.95}Eu_{0.05}Ba_{1-x}Sr_xZnSbO_6$ are truly due to the

symmetry change, not the concentration quenching. The emission intensity of $La_{1-x}Eu_xSrZnSbO_6$ increase along with the content of Eu^{3+} and no concentration quench was observed (see Fig. S5, ESI).

Conclusion

A series of double perovskites $LaBa_{1-x}Sr_xZnSbO_6$ were prepared by traditional solid state reactions. With substitution of Ba^{2+} by smaller Sr^{2+}, the structure symmetry of $LaBa_{1-x}Sr_xZnSbO_6$ lowered from $I2/m$ ($x \leq 0.4$) to $P2_1/n$ ($x \geq 0.6$) which was confirmed by the combination analyses of powder XRD and RED. Rietveld refinements on powder XRD suggest that Zn^{2+} and Sb^{5+} for all the title samples arranged in a completely rock-salt ordering, which was induced by the large size and charge differences between Zn^{2+} and Sb^{5+}. Sr^{2+}-doping leads to the increase of the average tilting angles of ZnO_6 and SbO_6 octahedra, which is helpful for improving the coordination environment of smaller Sr^{2+}. Additionally, Sr^{2+}-doping also leads to anisotropic shrinkage of the unit cell. The values of θ (defined as $c/[(a+b)/2]$) shows a minimum at $x = 0.4$, which is closely related to the change of tilt system from $a^-a^-c^0$ to $a^-a^-c^+$. The blue shift of CT bands of the excitation spectra of $La_{0.95}Eu_{0.05}Ba_{1-x}Sr_xZnSbO_6$ not only agrees with the evolution of the average <A-O> bond distances but also indicates the successful Sr^{2+}-doping. The emission intensities of $La_{0.95}Eu_{0.05}Ba_{1-x}Sr_xZnSbO_6$ increase along with the content of Sr^{2+}, which is consistent with the progressive modification of the local environment of A-site cations induced by the substitution of Ba^{2+} by smaller Sr^{2+}. The R/O ratios of $La_{0.95}Eu_{0.05}Ba_{1-x}Sr_xZnSbO_6$ were ~3.5, proving the Eu^{3+} cations located at a non-centrosymmetric site.

Electronic Supplementary Information: Tables for the cell parameters, atomic coordinates for $LaBa_{1-x}Sr_xZnSbO_6$ and $La_{0.95}Eu_{0.05}Ba_{1-x}Sr_xZnSbO_6$, Figures for electron diffraction of $LaBaZnSbO_6$, powder XRD patterns for $LaBa_{1-x}Sr_xZnSbO_6$ and $La_{0.95}Eu_{0.05}Ba_{1-x}Sr_xZnSbO_6$, final convergence of Rietveld refinements, emission spectra of $La_{0.95}Eu_{0.05}Ba_{1-x}Sr_xZnSbO_6$ excited by 394 nm and luminescence spectra for $La_{1-x}Eu_xSrZnSbO_6$ (x = 0.025, 0.05, and 0.08).

Acknowledgement

This work was financially supported by the Natural Science Foundation of China (Grants 91222106, 21171178), Natural Science Foundation Project of Chongqing (Grant 2014jcyjA50036) and the Fundamental Research Funds for the Central Universities (Grant CQDXWL-2014-005). We also acknowledge the support from the sharing fund of large-scale equipment of Chongqing University.

References

1 C. A. Paz de Araujo, J. D. Cuchiaro, L. D. McMillan, M. C. Scott, J. F. Scott, *Nature*, 1995, **374**, 627−629.

2 B. H. Park, B. S. Kang, S. D. Bu, T. W. Noh, J. Lee, W. Jo, *Nature*, 1999, **401**, 682−684.

3 B. W. Li, M. Osada, T. C. Ozawa, T. Sasaki, *Chem. Mater.*, 2012, **24**, 3111–3113.

4 R. J. Cava, B. Battlog, R. B. Van Dover, J. J. Krajewski, J. W. Wasczak, R. M. Fleming, W. F. Peck, L.W. Rupp, P. Marsh, A. C. James, L. F. Schneemeyer, *Nature*, 1990, **345**, 602.

5 R. J. Cava, B. Batlogg, J. J. Krajewski, R. Farrow, L.W. Rupp, A. E. White, K. Short, W. F. Peck, T. Kometani, Nature, 1988, **332**, 814 – 816.

6 N. Hayashi, T. Yamamoto, H. Kageyama, M. Nishi, Y. Watanabe, T. Kawakami, Y. Matsushita, A. Fujimori, M. Takano, *Angew. Chem. Int. Ed.*, 2011, **50**, 12547 –12550.

7 T. Ishihara, H. Matsuda, Y. Takita, *J. Am. Chem. Soc.*, 1994, **116**, 3801–3803.

8 M. J. Pitcher, P. Mandal, M. S. Dyer, J. Alaria, P. Borisov, H. J. Niu, J. B. Claridge, M. J. Rosseinsky, *Science*, 2015, **347**, 420-424.

9 C. Meneghini, R. Sugata, F. Liscio, F. Bardelli, S. Mobilio, D. D. Sarma, *Phys. Rev. Lett.*, 2009, **103**, 46403.

10 G. King, P. M. Woodward, *J. Mater. Chem.*, 2010, **20**, 5785–5796.

11 S. Vasala, M. Karppinen, *Prog. Solid State Chem.*, 2015, **43**, 1-36.

12 M. T. Anderson, K. B. Greenwood, G. A. Taylor, K. R. Poeppelmeier, Prog. *Solid State Chem.*, 1993, **22**, 197-233.

13 R. Shannon, *Acta Crystallogr., Sect. A: Cryst. Phys., Diffr., Theor. Gen. Cryst.*, 1976, **32**, 751–767.

14 *TOPAS, V4.1-beta*, Bruker AXS, Karlsruhe, Germany, 2004.

15 W. Wan, J. Sun, J. Su, S. Hovmöller, X. Zou, S. Hovmo, *J. Appl.Crystallogr.*, 2013, **46**, 1863−1873.

16 J. Su, E. Kapaca, L. Liu, V. Georgieva, W. Wan, J. Sun, V. Valtchev, S. Hovmöller, X. Zou, *Microporous Mesoporous Mater.*, 2014, **189**, 115−125.

17 H. Chen, J. Ju, Q. P. Meng, J. Su, C. Lin, Z. Y. Zhou, G. B. Li, W. L. Wang, W. L. Gao, C. M. Zeng, C. Tang, J. H. Lin, T. Yang, J. L. Sun, *J. Am. Chem. Soc.*, 2015, **137**, 7047−7050.18 C. J. Howard, B. J. Kennedy and P. M. Woodward, *Acta Crystallogr., Sect. B: Struct. Sci.*, 2003, **B59**, 463–471.

19 M. C. Blanco, S. A. Paz, V. M. Nassif, J. J. Guimpeld, R. E. Carbonio, *Dalton Trans.*, 2015, 44, 10860–10866.

20 M. C. Blancoa, J. M. De Paoli, S. Ceppi, G. Tirao , V. M. Nassif, J. Guimpel, R. E. Carbonio, *J. Alloys and Compd.*, 2014, **606**, 139–148.

21 T. K. Mandal, A. M. Abakumov, M. V. Lobanov, M. Croft, V. V. Poltavets, M. Greenblatt, *Chem. Mater.*, 2008, **20**, 4653–4660.

22 M. C. Knapp, P. M. Woodward, J. Solid State Chem., 2006, 179, 1076–1085.

23 A. M. Glazer, *Acta Crystallogr., Sect. A: Cryst. Phys., Diffr., Theor. Gen. Cryst.*, 1975, **31**, 756–762.

24 C. J. Howard, K. S. Knight, Kennedy, E. H. Kisi, *J. Phys. : Condens. Matter*, 2000, **12**, L677−L683.

25 M. Jansen, *Ang. Chem., Int. Ed. Eng.*, 1978, **17**, 137−137.

26 A. L. Sebastián, A. A José, S. Denis, A. Miguel, M. Angel, P. Vladimir, C. P. José, *J. Am. Chem. Soc.*, 2010, **132**, 14470–14480.

27 A.K. Ganguli, V. Grover, M. Thirumal, *Mat. Res. Bull.*, 2001, **36**, 1967–1975.

28 M. P. Attfield, P. D. Battle, S. K. Bollen, T. C. Gibb, R. J. Whitehead, *J. Solid State Chem.*, 1992, **100**, 37-48.

29 S. Nakamura and G. Fasol, *The Blue Laser Diode: GaN Based Light Emitters and Lasers;* Springer, Berlin, 1997.

30 X. F. Yi, R. H. Cong, Z. Y. Zhou, P. F. Jiang, W. L. Gao, T. Yang, *New J. Chem.*, 2014, **38**, 122-131.

31 Q. Q. Li, R. H. Cong, W. L. Gao, T. Yang, *J. Mater. Chem. C*, 2015, **3**, 6836-6843.

32 S. Ye, C.H. Wang, Z.S. Liu, J. Lu, X.P. Jing, *Appl. Phys. B–Lasers Opt.*, 2008, 91, 551–557.

33 X. Yin, Y. M. Wang, F. Q. Huang, Y. J. Xia, D. Y. Wan, J. Y Yao, *J. Solid State Chem.*, 2011, **184**, 3324–3328.

34 X. Q. Piao, K. Machida, T. Horikawa, H. Hanzawa, Y. Shimomura, N. Kijima, *Chem. Mater.* 2007, **19**, 4592-4599.

Table 1 Atomic coordinates, isotropic thermal displacement factors and site occupancies for $LaBaZnSbO_6$ and $LaSrZnSbO_6$ obtained from Rietveld refinements on powder XRD.

$LaBaZnSbO_6$	***x***	***y***	***z***	**Occupancy**	**B_{eq} (Å^2)**
Ba/La	0.500(3)	0	0.2484(6)	0.5/0.5	0.013(4)
Zn	0	0	0	1	0.013(1)
Sb	0	0	0.5	1	0.011(3)
O1	0.047(8)	0	0.249(5)	1	0.016(3)
O2	0.286(4)	0.227(4)	0.980(4)	1	0.016(3)

$LaSrZnSbO_6$	***x***	***y***	***z***	**Occupancy**	**B_{eq} (Å^2)**
La/Sr	0.999(2)	0.5253(2)	0.245(6)	0.5/0.5	0.0067(9)
Zn	0	0	0	1	0.005(1)
Sb	0	0	0.5	1	0.0023(8)
O1	0.065(6)	0.994(1)	0.245(6)	1	0.003(1)
O2	0.738(4)	0.264(5)	0.054(3)	1	0.003(1)
O3	0.194(6)	0.219(7)	0.974(3)	1	0.003(1)

Table 2 Selected interatomic distances (Å) and bond angles (º) for $LaBaZnSbO_6$ and $LaSrZnSbO_6$. Calculated bond valence sums for Zn^{2+} and Sb^{5+} are also given.

$LaBaZnSbO_6$			
La/Ba-O2 ×2	2.57(3)	Zn-O1 ×2	2.03(4)
La/Ba-O2 ×2	2.81(3)	Zn-O2 ×4	2.09(2)
La/Ba-O2 ×2	2.93(3)	BVS	2.23
La/Ba-O2 ×2	3.15(3)	Sb-O1 ×2	2.04(4)
La/Ba-O1 ×1	2.60(5)	Sb-O2 ×4	1.99(2)
La/Ba-O1 ×2	2.866(5)	BVS	4.99
La/Ba-O1 ×1	3.13(5)	Zn-O1- Sb	164.9
		Zn-O2- Sb	163.9
$LaBaZnSbO_6$			
La/Sr-O1	2.50(3)	Zn-O1 ×2	2.07(4)
La/ Sr-O1	2.67(1)	Zn-O2 ×2	2.08(3)
La/ Sr-O1	3.03(1)	Zn-O3 ×2	2.11(2)
La /Sr-O1	3.17(3)	BVS	2.13
La/ Sr-O2	2.46(3)	Sb-O1 ×2	1.99(4)
La/ Sr-O2	2.70(3)	Sb-O2 ×2	2.01(4)
La/ Sr-O2	2.88(3)	Sb-O3 ×2	1.99(2)
La /Sr-O3	3.52(3)	BVS	5.18
La/ Sr-O3	2.56(3)	Zn-O1- Sb	160.7
La/ Sr-O3	3.05(3)	Zn-O2- Sb	155.7
La/ Sr-O3	3.26(2)	Zn-O3- Sb	154.7

Graphical Abstract for

B-site ordered double perovskite $LaBa_{1-x}Sr_xZnSbO_6$ ($0 \leq x \leq 1$): Sr^{2+}-doping induced symmetry evolution and structure-luminescence correlations

Pengfei Jiang, Zhengyang Zhou, Wenliang Gao, Rihong Cong, and Tao Yang

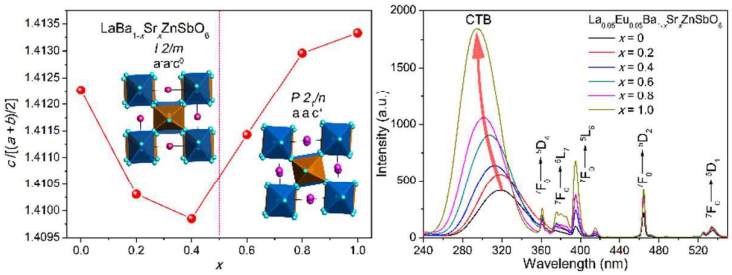

With Sr^{2+}-substitution, the ordered perovskite structure of $LaBa_{1-x}Sr_xZnSbO_6$ evolved from $I2/m$ to $P2_1/n$, together with a change of Eu^{3+}-luminescence.